

# The role of open volume defects in Mg-doped GaN studied by positron annihilation spectroscopy

S. Hautakangas and K. Saarinen

*Laboratory of Physics, Helsinki University of Technology, P.O.Box 1100, FIN-02150 Espoo, Finland*

L. Liskay\*

*Institut für Nukleare Festkörperphysik, Universität der Bundeswehr München, 85577 Neubiberg, Germany*

J. A. Freitas, Jr., and R. L. Henry

*Naval Research Laboratory, Washington D.C. 20375, US*

(Dated: April 7, 2005)

We have performed a systematic study of magnesium doped, co-doped and annealed MOCVD GaN films by positron annihilation spectroscopy. GaN:Mg films are free of detectable vacancy defects up to  $[\text{Mg}] \sim 3 \times 10^{18} \text{ cm}^{-3}$ , but at doping levels above  $10^{19} \text{ cm}^{-3}$  vacancies are observed. Two defects are identified:  $V_{\text{N}}\text{-Mg}_{\text{Ga}}$  pairs and vacancy clusters, where the amount of the missing atoms is estimated to be about 60. The defects have an inhomogeneous depth profile with a layer of higher defect concentration 100-500 nm below the surface. Thermal annealing dissociates the  $V_{\text{N}}\text{-Mg}_{\text{Ga}}$  pairs and the vacancy clusters, which migrate and form a homogeneous distribution of smaller clusters through the film. The identified defects play an important role in the electrical compensation and activation of the Mg acceptors in GaN films, and show correlations with results from transmission electron microscopy and photoluminescence studies.

## I. INTRODUCTION

The p-type doping of the gallium nitride (GaN) is one of the biggest challenges in GaN based device development. The n-type material is easily achieved by donor impurities doping e.g. by silicon or oxygen. Presently, the best impurity for p-type doping is magnesium, but the room temperature hole concentrations are generally limited to the moderate level of  $\sim 10^{17} \text{ cm}^{-3}$ .

Hydrogen is always present in epitaxial GaN films grown by metal organic chemical vapor deposition (MOCVD). The H present in the organo metallic precursors can passivate the Mg acceptors in the material. The H can be removed by post-growth annealing<sup>1</sup> at moderate temperature ( $\sim 800 \text{ }^\circ\text{C}$ ) or by low-energy electron beam irradiation<sup>2</sup> making the material p-type conductive. However, there is experimental evidence that nitrogen vacancy ( $V_{\text{N}}$ ) can be a compensating center for Mg acceptor.<sup>3,4</sup> The formation energies of  $V_{\text{N}}$  and  $\text{Mg}_{\text{Ga}}\text{-}V_{\text{N}}$  pair are low<sup>5</sup> in p-type material. The activation energy for  $V_{\text{N}}$  diffusion is controlled by Fermi energy.<sup>6</sup> In the midgap the charge state of  $V_{\text{N}}$  is +1 and the diffusion is unlikely to happen. In p-type GaN the N vacancy has a charge state +3 which is much more mobile.

Great effort has been put to the studies of large open volume defects like vacancy clusters and pinholes in Mg doped GaN. Liliental-Weber *et al.* has shown with transmission electron microscopy measurements that Mg dopants segregate in the planar defects.<sup>7</sup> These Mg atoms are likely to be electrically inactive. They have also shown that the Mg decoration of the hollow pyramidal defects correlates to the change of crystal polarity during growth.<sup>8</sup>

We use positron annihilation spectroscopy to investi-

gate the native defects in Mg-doped GaN films. The method is an effective tool for studying vacancy type defects in semiconductors (see e.g. Ref. 9). Because of the positron charge, it can be found in the region where the positive background is reduced. The positron is trapped by negative and neutral vacancies due to the missing positive ion core. The trapping increases the lifetime of the positron and narrows the momentum distribution of the positron-electron pair. These annihilation data can be used to distinguish between different vacancy-related defect types as well as to estimate the vacancy concentration with sensitivity in the range  $10^{16}\text{-}10^{19} \text{ cm}^{-3}$ . The momentum distribution of the electron at the vacancy can be measured directly in the energy distribution of the annihilation photons. This enables the identification of atoms neighboring the vacancy.

In our previous publication<sup>10</sup> we have shown that nitrogen vacancy is a compensating center in Mg doped GaN. The N vacancy can be removed by annealing at moderate temperature. The vacancy was identified as neutral  $\text{Mg}_{\text{Ga}}\text{-}V_{\text{N}}$  pair, which dissociates by thermal annealing leading to a diffusing nitrogen vacancy. In this paper we investigate further the nature of vacancy related defects in Mg doped, codoped and thermally annealed GaN films. In addition to nitrogen vacancy complexes, we also focus on larger vacancy clusters, which have been previously observed in Mg doped GaN.<sup>10,11</sup> These defects may also have influence on the compensation level of the material.

In Sec. II we describe the experimental set up and samples used in this study and Sec. III we present our results obtained with positron annihilation measurements. In Sec. IV we discuss the mechanism of electrical compensation as well as the effect of annealing and compare these results with those obtained by other measurement

methods. A summary of our results is given in Sec. V.

## II. EXPERIMENTAL DETAILS AND SAMPLES

### A. Samples

The experiments were performed on six epitaxial GaN films, referred to as Nos. 1-6, grown on a-plane sapphire substrates by MOCVD. Secondary-ion-mass-spectroscopy (SIMS) was employed to determine the total Mg, Si, H, O, and C concentrations in the films. The magnesium concentration of samples varies between  $0.25\text{-}9 \times 10^{19} \text{ cm}^{-3}$  and the  $[\text{Si}] = 0.13\text{-}8.4 \times 10^{18} \text{ cm}^{-3}$ . In addition, the sample #2 has hydrogen concentration of  $4 \times 10^{18} \text{ cm}^{-3}$  and  $[\text{O}] = 1 \times 10^{17} \text{ cm}^{-3}$ . Samples no. 3 and 4 are intentionally codoped with Si, the other samples have moderate Si concentration coming from the reactor walls during growth. Note that the samples #2 and #6 are the same as studied in Ref. 12 (samples 4 and 1 therein). The post-growth heat treatments were done by rapid thermal annealing (RTA) at  $980 \text{ }^\circ\text{C}$  and in the case of Si co-doping at  $1000 \text{ }^\circ\text{C}$ . As can be seen the Mg concentration is over two orders of magnitude bigger than hole concentration in sample #2. A p-type Mg-doped GaN sample grown by molecular beam epitaxy (MBE) was used as a vacancy free reference sample.<sup>13</sup>

The photoluminescence (PL) experiments carried out at 6K was excited by the 325 nm line of a HeCd laser at a power density of  $\sim 8 \text{ W/cm}^2$ . The light emitted by the samples were dispersed by a double-grating spectrometer fitted with 1800 groves/mm. A UV-extended GaAs photomultiplier coupled to a computer-controlled photon counter was used for data acquisition. The PL spectra were corrected for the instrumental response by normalization to the throughput of a broadband calibrated lamp. To illustrate the optoelectronic properties of Mg doped samples we represented in Fig. 1 the PL spectra of three GaN films (indicated as S#a, S#b, and S#c) doped with increasing concentration of Mg. The relative redshift of the peak positions with increasing doping level has been attributed to potential fluctuation induced by charged donor/acceptor centers and to the incorporation of deep donors, respectively.<sup>14,15</sup>

### B. Positron Doppler spectroscopy

After implantation into the material the positron loses its energy and reaches a thermal equilibrium with surroundings in a few picoseconds and starts to diffuse. Negatively and neutrally charged defects, especially vacancies can trap positron. Finally, the positron annihilates with electron into two 511  $\gamma$ -quanta. The 511 keV annihilation line is broadened because of the momentum of the electron. By studying the Doppler shift of the annihilation energy the information about the electron configuration at the annihilation site can be revealed.

TABLE I: The Mg and Si concentrations measured by secondary ion-mass spectrometry in studied GaN layers. The hole concentrations were determined with Hall measurement<sup>12</sup> and in the case of reference sample with capacitance-voltage measurements. RTA stands for rapid thermal annealing and SITU means that samples were annealed in the growth reactor.

Sample number	Mg conc. $\times 10^{19} \text{ cm}^{-3}$	Si conc. $\times 10^{17} \text{ cm}^{-3}$	Hole conc. $\times 10^{17} \text{ cm}^{-3}$	Annealing temp. $^\circ\text{C}$
#1	4.0	1.3	-	No anneal.
#2	4.0	1.3	1.7	980/RTA
#3	7.3	72	-	No anneal.
#4	9.0	84	-	1000/RTA
#5	1-2	5-6	-	800/SITU
#6	0.25	5-6	highly resistive	800/SITU
ref. <sup>16</sup>	-	-	$\sim 10$	No anneal.

The energy distribution of annihilated positron-electron pairs is characterized by S and W parameter (see e.g. Ref. 17). S parameter measures counts of the central part of the 511 keV peak and the W parameter describes the counts in the wing areas of the peak. Thus the S parameter represents annihilations with valence electrons with longitudinal momentum component of  $p_L \leq 3.7 \times 10^{-3} m_0 c$  and W parameter describes the annihilations with high momentum core electrons,  $11 \times 10^{-3} m_0 c \leq p_L \leq 29 \times 10^{-3} m_0 c$ . At a vacancy the electron momentum is locally decreased, which leads to the narrowing of the energy distribution of annihilation photons. This can be characterized as higher S parameter and lower W parameter than in bulk material.

The valence annihilation parameter S at a given energy is a linear superposition of the values  $S_i$

$$S = \eta_b S_b + \sum_{i=1}^N \eta_i S_i, \quad (1)$$

where the  $S_i$  and  $S_b$  are characteristic S parameter values for annihilations at the different positron states, and weighting factors  $\eta_i$  and  $\eta_b$  are the fractions of positron annihilations at each state. The letter b denotes the annihilations of delocalized positrons. Similar equation holds for the W parameter. If only one vacancy type defect trapped the positron, the experimental S and W parameter would be linear combinations of values  $(S_b, W_b)$  and  $(S_V, W_V)$ , which correspond to annihilations of free positron in defect free lattice and annihilations of positron trapped at vacancies, respectively. The measured S and W parameters would then fall on a line connecting the points  $(S_b, W_b)$  and  $(S_V, W_V)$  in the S-W plot. This analysis enables to distinguish between different annihilation sites.

We use a low energy positron beam. The positrons emitted from <sup>22</sup>Na source with initial energies up to several hundred keV are moderated using W foil. After moderation positrons are accelerated to the energies be-

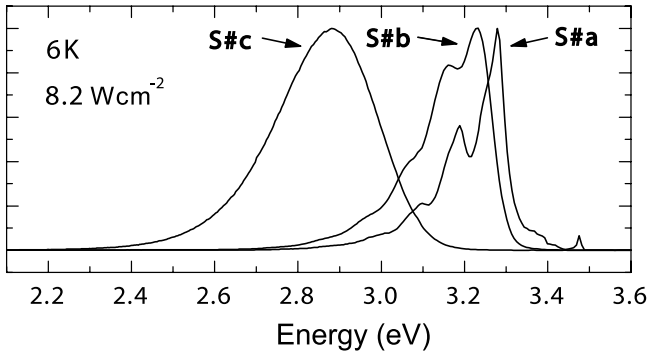


FIG. 1: Normalized low temperature PL spectra of three GaN:Mg epitaxial films deposited by MOCVD on a-face sapphire substrates. Note the line shape change and the red-shift of the peak position with increasing Mg concentration, from  $2.5 \times 10^{18}$  to  $7 \times 10^{19} \text{ cm}^{-3}$ . These samples have been post-growth thermal anneal at  $950 \text{ }^\circ\text{C}$ . The spectra are corrected for instrumental response.

tween 0-30 keV. The annihilation radiation is detected with high resolution (1.2 keV at 511 keV) germanium detectors.

### C. Positron lifetime spectroscopy

The trapping of positrons at the vacancy increases the average lifetime of the positron because the electron density is reduced at the vacancy. By measuring the lifetime one can distinguish between different open volume defects and estimate their concentrations. Pulsed low-energy positron beam enables lifetime measurements in thin semiconductor layers. The positron lifetime is measured as a time interval between an annihilation  $\gamma$ -photon and beam pulse edge, where the pulsing is done after the beam moderation. A couple of millions of counts are measured to the peak to have reliable information about the defects in the samples.

To find the average lifetimes and to decompose the lifetime spectra the resolution has to be taken into account. After subtracting the background the lifetime spectra can be analyzed as a sum of exponential decay components  $n(t) = \sum_i I_i \exp[-\lambda_i t]$ . The resolution function is a sum of three Gaussian distributions. The center of mass of the lifetime spectrum  $\tau_{\text{ave}} = \sum_i I_i \tau_i$  increases with increased positron trapping into vacancies.

## III. POSITRON STUDIES

### A. Doppler results

Figure 2 shows the S parameter as a function of incident positron energy in samples with different Mg concentrations. The reference level corresponding to vacancy free lattice is represented by the dashed line. In the lat-

tice, the positron wave function is delocalized. The annihilation from a bulk state gives the most broadened momentum distribution, which can be seen as a low S parameter. The vacancy free S parameter level as well as the bulk lifetime ( $\tau_b = 160 \pm 5 \text{ ps}$ ) in GaN are well known on the basis of previous studies.<sup>10</sup> Here we use a MBE GaN:Mg reference sample, which has the same positron lifetime as a defect free GaN lattice according to earlier measurements.<sup>10,18</sup>

In Fig. 2 the top axis shows the mean implantation depth of a positron related to the used acceleration voltage. The behavior of S parameter can be divided in three different region: (1) Surface, (2) layer and (3) substrate. At low acceleration voltage ( $< 2 \text{ keV}$ ) the penetration depth of positrons is low and they can diffuse back to the surface. The electron density is reduced at the surface, resulting in a narrower annihilation line, which is observed as a higher S parameter. At higher acceleration voltage (5-20 keV) the S parameter characterizes the GaN layer. At even higher energies the S parameter is decreasing because the positrons are implanted to the sapphire substrate, where the electron momentum is higher. The measured S parameter is hence a linear combination of individual S parameter of each region with respective weighting factors  $\eta_i$  (see Eq. 1).

To study the effect of Mg doping one has to focus in the region of 250-500 nm (Fig. 2). The sample containing the lowest Mg concentration has the same S parameter level as in bulk GaN. No vacancies are thus detected. On the other hand, the S parameter is  $\sim 0.466$  for the sample with Mg concentration of  $1-2 \times 10^{19} \text{ cm}^{-3}$ , and  $S \sim 0.473$  for sample #1 with highest Mg concentration. As can be seen the S parameter levels of samples have a clear order depending on the Mg content. Higher S parameter value is a finger print of vacancy type defect. At the vacancy the electron density is decreased and the annihilation line is narrower, yielding higher S parameter than in the bulk lattice. Hence, positrons reveal increased trapping in vacancy type defects with higher Mg concentrations.

GaN:Mg samples are often used as a vacancy free reference samples because the existing vacancies are in positive charge state and hence cannot trap positrons. The data of Fig. 2 indicates, however, that at very high Mg concentrations vacancy-related defects acting as positron traps are created.

Figure 3 shows the low-momentum parameter S as a function of incident positron energy at room temperature for both unannealed and annealed GaN:Mg with Mg concentration of  $4 \times 10^{19} \text{ cm}^{-3}$  and for the reference sample. The S parameter for unannealed sample #1 measured at 580 K is also represented. At low positron acceleration energies (0-2 keV) the S parameter of all samples is high due to the annihilations at surface states and decreases with increasing positron energies. Deeper probing (50-260 nm) of the unannealed GaN:Mg sample shows that the S parameter increases and reaches the plateau with constant value  $S \approx 0.473$  at 300 K and  $S \approx 0.515$  at 580 K, in the depth range between 260-790 nm. Excluding

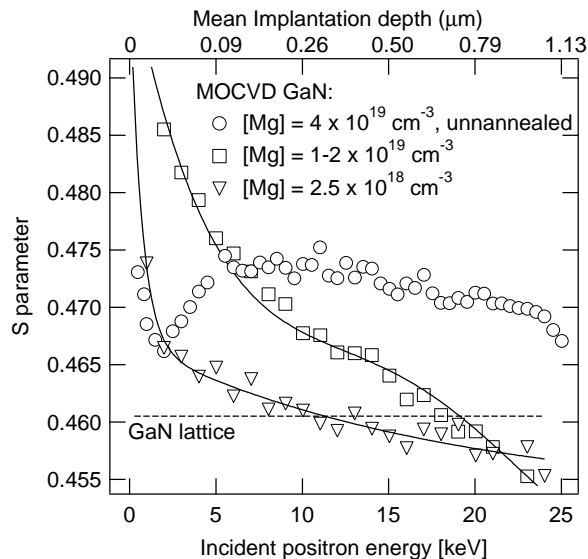


FIG. 2: The valence annihilation parameter  $S$  as a function of incident positron energy in GaN layers. The samples were annealed at  $800^\circ\text{C}$  except the one with highest Mg concentration. The dashed line represents the  $S$  parameter level of annihilations of delocalized positrons in the GaN lattice. The top axis indicates the mean implantation depth of incident positron. The solid lines are to guide the eye.

the surface, the  $S$  parameter of the annealed sample has a constant value  $S \approx 0.465$ . At positron energies  $> 20$  keV the  $S$  parameter starts to decrease due to the annihilations at  $\text{Al}_2\text{O}_3$  substrate.

$S$  parameter values higher than the bulk level indicate the presence of vacancy type defects (Fig. 3). It is evident from the experiment that the high measuring temperature makes the trapping at vacancies more effective. Right below the surface the  $S$  parameter of the unannealed sample has a local minimum, which corresponds to a region with lower vacancy concentration. After annealing the vacancy signal is still evident, but the profile is homogeneous. Comparing Figs. 2 and 3 one can deduce that high Mg content generates a vacancy profile, where the lower vacancy concentration is below surface and it increases deeper into the layer.

The temperature behavior of the valence annihilation parameter  $S$  is shown in the Fig. 4. The  $S$  parameter level for vacancy free p-type reference sample is indicated with dashed line. At high temperatures ( $> 300$  K) the  $S$  parameters of samples #1 and #2 are clearly higher than that of the reference sample. At  $600$  K the  $S$  parameter of unannealed GaN:Mg sample reaches a value of  $S \approx 0.513$  and the data of the annealed sample increase up to  $S \approx 0.481$ . The  $S$  parameters of co-doped samples are also higher than that of the reference sample indicating positron trapping at the vacancies.

In addition to vacancies, positrons trapping by negative ions can also be detected. Positrons are localized with an energy of typically  $0.01$ - $0.1$  eV around negative

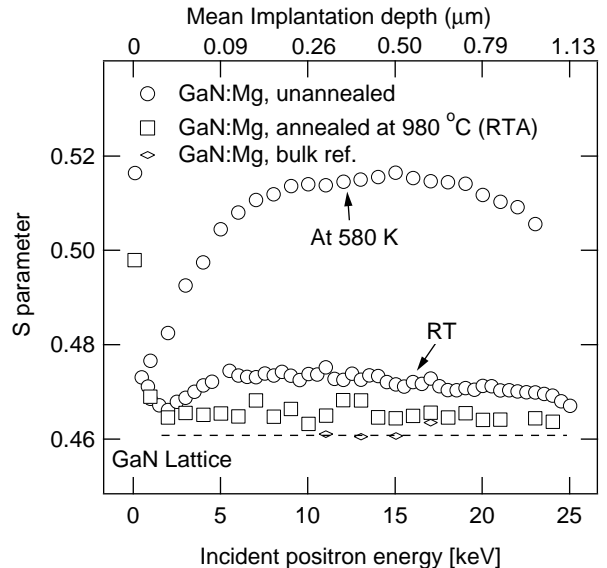


FIG. 3: The valence annihilation parameter  $S$  as a function of incident positron energy in annealed and unannealed GaN:Mg sample with Mg concentration of  $4 \times 10^{19} \text{ cm}^{-3}$ . The p-type GaN:Mg is used as vacancy free reference. The top axis indicates the mean penetration depth.

ions. Due to the low binding energy positrons can escape from the localized state with increasing temperature. The electron density around the negative ion is almost the same as in the bulk, leading to similar  $S$  parameter and positron lifetime values. In order to distinguish between the annihilations at the ion from that in the bulk, the temperature dependence of the positron trapping is studied. In practice, the negative ions are detected through decreasing  $S$  parameter and average lifetime when the sample temperature is decreased.

The samples have two competing positron traps based on the measurements as a function of temperature (Fig. 4). At low temperature the positrons get trapped by defects without open volume and thus less annihilations take place at vacancies. The candidate for this process is the negative ion. The competing positron traps in Mg doped GaN were also observed in a previous work<sup>10</sup>, where the negative ion is attributed to  $\text{Mg}_{\text{Ga}}$  acceptor. Another type of shallow positron trap is dislocation without open volume, as observed in n-type GaN.<sup>19</sup>

## B. Lifetime results

Figure 5 shows the average lifetime  $\tau_{ave}$  as a function of incident positron energy in the unannealed GaN:Mg sample measured at  $300$  K. At the surface the average lifetime is high due to the low electron density.  $\tau_{ave}$  is lowest with positron energy of  $2$  keV and increases to the constant value of  $\tau_{ave} = 185$  ps in the range of  $100$ - $500$  nm. Deeper probing in the sample  $\tau_{ave}$  decreases

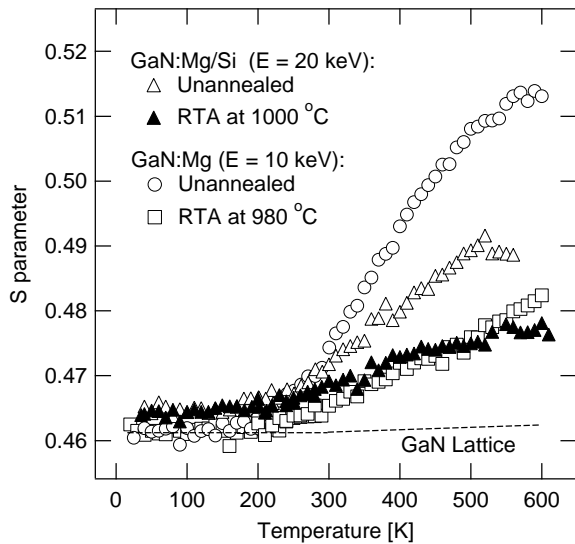


FIG. 4: Valence annihilation parameter  $S$  as a function of measuring temperature. The incident positron energy was chosen high enough to make sure the annihilations arising from the surface are excluded.

due to the annihilations in the sapphire substrate. As can be seen in Fig. 5 there is a region of lower vacancy concentration below the surface in agreement with the result obtained by Doppler measurement (Fig. 3).

The average lifetime of a positron as a function of temperature is shown in Fig. 6. At low temperature ( $T = 85$  K)  $\tau_{ave} \approx 150$  ps is equal to the lifetime of the defect-free lattice, similarly as seen in the Doppler experiment in Fig. 4. Therefore, positrons are trapped at shallow traps (negative ions, dislocations) preventing the annihilation at vacancies. With increasing temperature the average lifetime increases because positrons escape from the shallow trap and larger fraction of them are annihilating at vacancies. The high temperature enhances the positron trapping at vacancy type defects and at 540 K the average lifetime increases up to 223 ps.

### C. Identification of vacancies

To analyze the annihilation parameters independently of the vacancy concentration the core annihilation parameter  $W$  can be shown as a function of valence annihilation parameter  $S$ . Figure 7 shows the  $W$  vs.  $S$  plot measured in the annealed and unannealed sample. Both of these parameters were normalized with those measured for the GaN lattice. In the case of a single type of vacancy defect the measured  $S$  and  $W$  parameters fall on the straight line connecting the bulk value ( $S_b, W_b$ ) and defect related value ( $S_d, W_d$ ). The slope characterizes the defect species and does not depend on the concentration of the vacancy.

Figure 7 also shows the characteristic  $S$  and  $W$  pa-

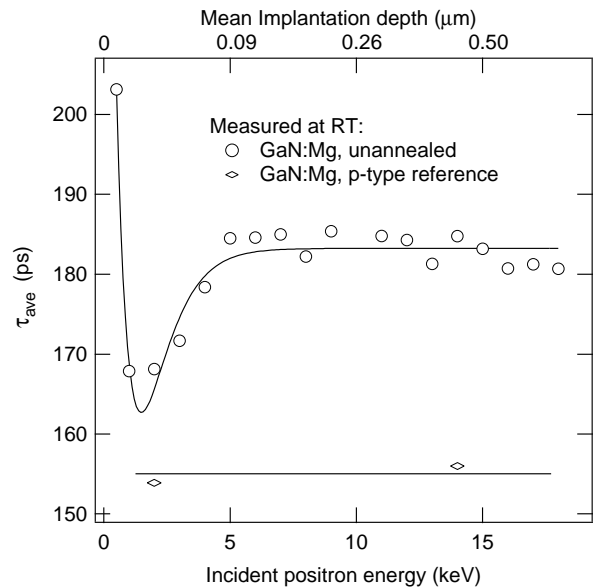


FIG. 5: The average lifetime of positrons as a function of incident positron energy in the unannealed GaN:Mg sample. The p-type Ga:Mg sample is used as a vacancy free reference. The solid line is to guide the eye.

rameters for gallium vacancy ( $V_{Ga}$ ) as obtained in Ref. 20. The slope of  $S$ - $W$  plot for the as-grown sample #1 is almost the same as measured before<sup>21</sup> for vacancy cluster. Furthermore, the slope of  $S$ - $W$  plot is constant, which means that single vacancy type defect dominates the Doppler broadened spectrum. The change in relative  $S$  parameter ( $S/S_b \sim 1.1$ ) of the unannealed sample is typical for vacancy clusters and much larger than expected for monovacancies.

After annealing, the change in the relative  $S$  parameter is more moderate ( $S/S_b \sim 1.045$ ). This  $S$  parameter is close to those determined for the native Ga vacancy.<sup>20</sup> Again the slope is constant indicating a single dominant vacancy defect type. However, the slope differs from the one before annealing, which shows that the dominant type of vacancy defect changes. Since the ( $S, W$ ) parameter become closer to that of  $V_{Ga}$ , we conclude that the size of the vacancy cluster decreases with thermal annealing.

The co-doping of GaN:Mg samples with Si atoms generates also vacancy related defects as observed in Fig. 4. Before annealing they have the characteristic slope in  $S$ - $W$  plot (Fig. 7) revealing the existence of vacancy clusters. We conclude that the annealing changes the slope, similarly as in the Mg doped samples #1 and #2. The annealing makes these clusters to convert to smaller size vacancy defects with annihilation parameters close to those of  $V_{Ga}$ .

To identify vacancies and to study their profile in the GaN:Mg sample #1 (see Figs. 2,3,5) the positron lifetime measurement with two different acceleration voltage has been performed (Fig. 8). The measurement voltages

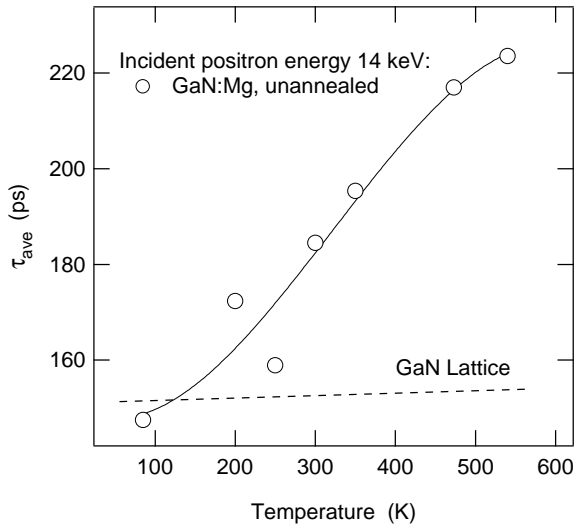


FIG. 6: The average positron lifetime of unannealed GaN:Mg sample as a function of measuring temperature. The incident positron energy was 14 keV. The solid line is to guide the eye.

were 2 keV and 14 keV where maximum effects in depth profile can be expected (Figs. 3,5). Figure 8 also shows the lifetime spectrum of MBE grown GaN:Mg reference sample, which was measured at 300 K using acceleration voltage of 14 keV to minimize annihilation events at the surface. Only one lifetime component can be distinguished from the spectrum of the reference sample with the value of  $\tau_{\text{bulk}} = 155 \pm 1$  ps. This is consistent with theoretical calculations<sup>22</sup>, where  $\tau_{\text{bulk}} = 156$  ps, and it is similar to previously measured value for positron annihilation in the GaN lattice.<sup>10,18</sup>

The decompositions of the lifetime spectra are shown in Table II. In the unannealed sample #1 three different lifetimes components are found. The smallest is  $\tau_1 \approx 70$  ps which is related to positron annihilations in the delocalized state. In the presence of open volume defects the lowest lifetime is clearly smaller than the bulk lifetime. This happens because of the trapping: The free positron annihilation has to take place before trapping into the vacancy.

The spectrum of unannealed GaN:Mg measured at 14 keV (Fig. 8) reveals high intensities of two vacancy related lifetimes. The lower is  $\tau_2 = 180$  ps and the higher is  $\tau_3 = 435$  ps, which are the same values as detected previously<sup>10</sup>. The shorter lifetime  $\tau_2 = 180$  ps is clearly longer than lifetime in the GaN lattice. On the other hand it is shorter than that obtained for gallium vacancy  $\tau_{V_{\text{Ga}}} = 235 \pm 5$  ps.<sup>20</sup> The natural choice is then the nitrogen vacancy. The isolated  $V_{\text{N}}$  is positive and cannot trap positrons, so the  $V_{\text{N}}$  has to be neutralized with impurity, namely with the Mg atom. The formation energy of  $V_{\text{N}}\text{-Mg}_{\text{Ga}}$ -complex is calculated to be small in p-type material.<sup>5,20</sup> The lifetime  $\tau_2$  is the same as reported previously<sup>10</sup>, where the  $\tau_2 = 180$  ps is connected to the  $V_{\text{N}}\text{-Mg}_{\text{Ga}}$ -complex by studying the chemical en-

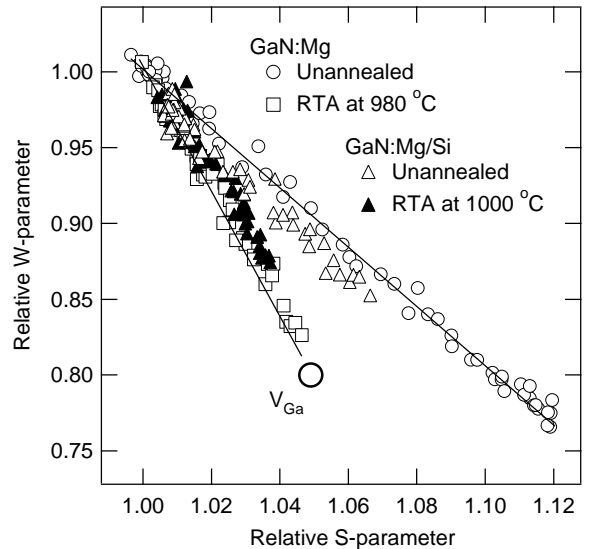


FIG. 7: The core annihilation parameter  $W$  as a function of valence annihilation parameter  $S$  measured at different temperatures.  $V_{\text{Ga}}$  represents positron annihilation parameters at Ga vacancy. Note, that the data are the same as in Fig. 4.

vironment of the vacancy with the Doppler broadening measurement. The electron configuration at the site of  $V_{\text{N}}$  is different depending on the neighborhood of the vacancy. The replacement of Ga atom by Mg atom was verified by reduced counts in the high momentum part of the annihilation energy.<sup>10</sup> Mg does not have  $3d$  electrons with high momenta. We thus attribute the lifetime component of 180 ps to positron annihilation at the  $V_{\text{N}}\text{-Mg}_{\text{Ga}}$  complex.

The longer lifetime component  $\tau_3 = 435$  ps is so large that it cannot arise from single mono vacancies. The lifetime of 435 ps is hence attributed to a vacancy cluster. The size of the vacancy cluster is discussed in more details below.

Interestingly the Doppler measurement and the  $(S,W)$  plot reveals only one vacancy type defect in the unannealed GaN:Mg, namely the vacancy clusters, whereas the decomposition of the lifetime spectra of the same sample yields two vacancy related lifetimes. We think that this behavior is related to the sensitivity of the  $S$  vs.  $W$  plot. Since the  $S$  and  $W$  parameters are dominated by the annihilations at the vacancy cluster, the  $V_{\text{N}}\text{-Mg}_{\text{Ga}}$ -complex is not revealed in the  $(S,W)$  plot since its momentum distribution is almost the same as in the bulk lattice.

In summary, positrons reveal two vacancy defects in as-grown unannealed GaN:Mg: (i) the  $V_{\text{N}}\text{-Mg}_{\text{Ga}}$  complex and (ii) and the vacancy cluster. The concentration of  $V_{\text{N}}\text{-Mg}_{\text{Ga}}$ -complexes increases with increasing Mg concentration and cluster formation are observed only for Mg doping levels of  $\geq 10^{19} \text{ cm}^{-3}$ . After thermal annealing vacancies are still detected, but their open volume is smaller and their annihilation parameters are close to

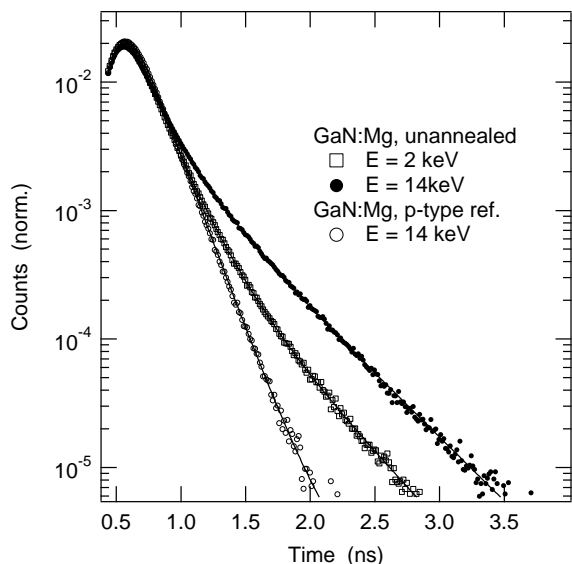


FIG. 8: Positron lifetime spectra in the unannealed GaN:Mg sample measured with two different positron energies at 540 K. The Mg-doped MBE grown p-type sample is shown as a vacancy free reference. The area of each spectrum was scaled to 1. Solid lines are the fitting results of respective spectra.

those of  $V_{\text{Ga}}$ . We attribute these to smaller vacancy clusters which are formed by dissociation of the larger vacancy clusters during the thermal annealing process.

#### D. Vacancy cluster size and saturation lifetime

It has been shown that the positron lifetime at vacancy clusters is sensitive to the size of the clusters.<sup>23,24</sup> To estimate the size of the open volume with the positron lifetime of 435 ps we calculate the positron lifetimes theoretically. For the positron states we use the conventional scheme with the local density approximation (LDA) for electron-positron correlation effects and the atomic superposition method in the numerical calculations.<sup>25,26</sup> The positron annihilation rate  $\lambda$  is

$$\tau^{-1} = \lambda = \pi r_0^2 c \int d\mathbf{r} |\psi_+(\mathbf{r})|^2 n_-(\mathbf{r}) \gamma [n_-(\mathbf{r})], \quad (2)$$

where  $n_-$  is the electron density,  $\psi_+(\mathbf{r})$  the positron wave function,  $r_0$  the classical electron radius,  $c$  the speed of light and  $\gamma$  is the enhancement factor, for which we use the interpolation by Boronski and Nieminen.<sup>27</sup> The positron state was solved in a 216 atom supercell, in vacancy clusters up to the size of 62 missing atoms (Fig. 9).

As can be seen in Fig. 9 the positron lifetime starts to saturate above 400 ps when the cluster includes more than 30  $V_{\text{Ga}}-V_{\text{N}}$  vacancy pairs. This is the consequence of the reduced electron density at the annihilation site.

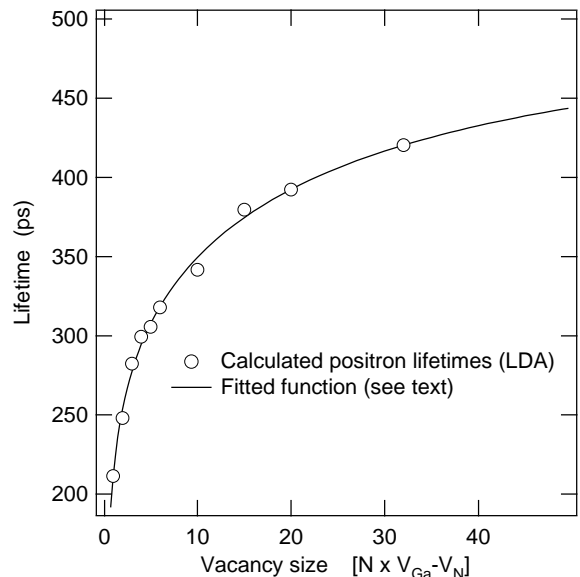


FIG. 9: The calculated positron lifetime as a function of the number of vacancy pairs. The solid line is a fit of a function, where the electron density  $n$  is inversely related to the vacancy cluster size.

The solid line in Fig. 9 represents the annihilation rate

$$\lambda = \tau^{-1} = (2 + Ae^{-Bn^{1/3}} + Ce^{-Dn^{1/3}}) \times 10^9 \text{ s}^{-1}. \quad (3)$$

The electron concentration  $n$  is inversely related to vacancy size  $N$ .  $A - D$  are fitting parameters. The function has a saturation lifetime 500 ps, which is the lifetime of the negative positronium atom, similarly as in the Brandt-Reinheimer formula.<sup>28</sup>

The electron density in a vacancy cluster plays a crucial role when determining the annihilation rate of a positron. We motivate the Eq. (3) in the following way. Ga atom is much bigger than  $N$ , and the positron probes mainly the electron density of a Ga atom. The electron density of Ga atom decreases exponentially with the radial distance  $r \propto N^{1/3}$ . At small cluster sizes positrons annihilate with both Ga ( $4s, 4p$ ) valence electrons and Ga ( $3d$ ) core electrons. In larger vacancy clusters the annihilation with the valence electrons strongly dominates. Hence, the fitted sum of two exponential functions can be thought as an annihilation with two different electron shells, which is controlled by the size of the vacancy cluster. As seen in Fig. 9, the simple scaling of Eq. (3) reproduces very well the positron lifetimes calculated with the atomic superposition method (Eq. (2)). The result of Fig. 9 is quantitatively similar to the behavior of the calculated positron lifetime in Fe vacancy clusters.<sup>29</sup> This means that the number of missing Ga atoms determines the positron lifetime.

The experimental positron lifetime of 435 ps is close to the saturation value of the curve represented in Fig. 9, but yet smaller than the  $n \rightarrow 0$  limit of 500 ps of the Brandt-Reinheimer formula.<sup>28</sup> The theoretical limit

TABLE II: Decomposed lifetimes of the unannealed GaN:Mg sample at two different positron energies. Background reduction was 0.3 % 500 ps at 14 keV and 5-6 % 350 ps extra component at 2 keV. The latter is arising from surface annihilations and is hence dependent on the measuring temperature. The defect concentrations are determined from the decomposed lifetimes by applying the positron trapping model (Eqs. 4-6).

Sample	Positron energy keV	Temperature K	$\tau_{ave}$ $10^{-9}$ s	$\tau_1/I_1$ ps/%	$\tau_2/I_2$ ps/%	$\tau_3/I_3$ ps/%	Vacancy conc. $\times 10^{17} \text{cm}^{-3}$	Cluster conc. $\times 10^{15} \text{cm}^{-3}$
Unann.	14	540	223(1)	70(2)/27(1)	183(3)/45(1)	435(3)/28(1)	2.7	4.5
	2	540	159(1)	71(4)/27(2)	173(3)/68(2)	438(9)/5(1)	1.9	0.5

value of 500 ps has been experimentally observed in other GaN:Mg samples,<sup>10</sup> as well as in deformed Si<sup>30</sup> or GaAs.<sup>29</sup> These comparisons suggest that the lifetime of 435 ps has not yet reached the saturation regime as a function of the vacancy cluster size. Therefore, we attribute it to clusters where about 60 atoms (30 GaN molecules) are missing (cluster radius of  $\sim 5$  Å).

### E. Vacancy concentrations

The positron trapping into the vacancies depends on the measuring temperature and the vacancy charge state.<sup>31</sup> Positive vacancies cannot trap positron due to the Coulombic repulsion. Neutral and negative vacancies can trap positrons with the trapping rate

$$\kappa = \mu c, \quad (4)$$

where  $\mu$  and  $c$  are the trapping coefficient and the defect concentration, respectively. In the case of large vacancy clusters the trapping is limited by positron diffusion and the trapping rate is

$$\kappa = 4\pi r D_+ c, \quad (5)$$

where the  $r$  is the radius of the void and  $D_+$  is the diffusion constant of the positron.

The vacancy concentrations can be calculated from the trapping rate  $\kappa$ . On the basis of the intensities of the lifetime components one can deduce  $\kappa_V$  and  $\kappa_{cl}$ . The concentrations are calculated from equations  $[V_{N-Mg_{Ga}}] = N_{at} \kappa_V / \mu_V$  and  $[V_{cl}] = N_{at} \kappa_{cl} / \mu_{cl}$  for vacancy and cluster type defects, respectively.  $N_{at} = 8.78 \times 10^{22} \text{cm}^{-3}$  is the atomic density of the material and  $\mu_V = 10^{15} \text{s}^{-1}$  is the trapping coefficient for the transition limited trapping i.e. for mono vacancies. In the case of vacancy cluster the size is  $r = 5$  Å (estimated above) and  $D_+ = 1 \text{cm}^2/\text{s}$  giving  $\mu_{cl} = 4\pi r D_+ N_{at} = 5.5 \times 10^{16} \text{s}^{-1}$ .

The model applied here includes two different types vacancy defects and no detrapping, i.e., no positron escaping from the trap. This is reasonable because the measuring temperature is 540 K and the thermal energy is high enough to prevent the trapping at shallow traps, i.e., negative ions or dislocations. All different positron states were considered to be non-interacting.  $\kappa_V$  and  $\kappa_{cl}$

can be calculated with the help of intensities  $I_2$  and  $I_3$

$$\begin{cases} I_2 = \frac{\kappa_V}{\lambda_b - \lambda_V + \kappa_V + \kappa_{cl}} \\ I_3 = \frac{\kappa_{cl}}{\lambda_b - \lambda_{cl} + \kappa_V + \kappa_{cl}} \end{cases}, \quad (6)$$

where  $\lambda_b = \tau_b^{-1} = (155 \text{ps})^{-1}$ ,  $\lambda_V = \tau_V^{-1} = (180 \text{ps})^{-1}$  and  $\lambda_{cl} = \tau_{cl}^{-1} = (435 \text{ps})^{-1}$ .  $I_2$  and  $I_3$  are the intensities of  $\tau_2$  and  $\tau_3$ , respectively, and they are listed in the Table II. As can be seen from Table II the vacancy as well as the cluster concentrations are lower near the surface. The decrease in  $V_{N-Mg_{Ga}}$  concentration is small while the cluster concentration is an order of magnitude smaller close to the surface. The inhomogeneous vacancy concentration, observed both in S parameter and in the average positron lifetime, evidently arises from the vacancy cluster concentration.

## IV. DISCUSSION

### A. Mg doping, electrical compensation and vacancy defects

The electrical inactivity of Mg acceptors in GaN:Mg is generally associated to the passivation induced by hydrogen atoms. MOCVD growth uses Ga atoms precursors in the form of trimethylenegallium (TMGa) and the residual H in the growth environment is readily available to passivate the Mg acceptor. The migration barrier for H is low, and the annealing at moderate temperatures activates the Mg acceptors by dissociating the H from the Mg atoms. The binding of hydrogen to Mg ions and its dissociation have been observed by local vibrational mode spectroscopy<sup>32,33</sup> and the results are generally in agreement with theoretical calculations.<sup>34</sup>

The high level of Mg doping (above  $10^{19} \text{cm}^{-3}$ ) seems to have competing mechanisms for Mg deactivation. The  $V_{N-Mg_{Ga}}$  pairs observed here by positron spectroscopy compensate Mg atoms making the material more resistive. The post-growth annealing decreases the concentration of  $V_{N-Mg_{Ga}}$  complexes, which can be interpreted as the dissociation of the  $V_{N-Mg_{Ga}}$  pairs.<sup>10</sup> This process leads to electrically active Mg ions, in an analogous manner as in the case of H passivation. Furthermore, the vacancy clusters observed here may also have a role in the electrical compensation of Mg doping.

Z. Liliental-Weber *et al.* have studied the formation of pyramidal defects in Mg doped GaN. These defects are associated with inversion domains<sup>8,35</sup>, and accordingly to TEM measurement they are hollow. The defects are further decorated by Mg<sup>7,36</sup> which suggests that they are important for the compensation of the material. Comparing this with the present positron studies, we can conclude that the high S parameter value as well as the high intensity of the long positron lifetime component correlates well with the TEM results. In addition, the inhomogeneous cluster profile is in good agreement with the typical TEM images,<sup>37</sup> suggesting strongly that the profile of open volume (detected by positrons) corresponds to that of the pyramidal defects. On the other hand, the size of the vacancy clusters detected here (60 atoms, 0.5 nm radius) is smaller than the typical size of the pyramidal defects observed by TEM (1 - 10 nm). The positron spectroscopy, as a technique with atomic-size resolution, is perhaps sensitive primarily to smaller vacancy clusters as reported by TEM experiments, although the origin of both observations could be similar, i.e. the inversion domain triggered by Mg doping.

The positron annihilation data allow to estimate quantitatively the Mg compensation by vacancy defects. The concentration of passivated Mg acceptors can be estimated by taking the value of  $1.25m_e$ <sup>38</sup> for the effective hole mass in GaN and 0.2 eV for ionization energy  $E_a$  for the acceptors. By simple Fermi statistics<sup>38</sup> one can find the level of ionized Mg to be  $3.3 \times 10^{18} \text{ cm}^{-3}$ .<sup>39</sup> The concentration of  $V_N\text{-Mg}_{Ga}$  complexes is  $2 - 3 \times 10^{17} \text{ cm}^{-3}$  according to the analysis of the positron data (Table II). This defect thus contributes to the electrical deactivation of Mg, but its role may be only about 10% of the total compensation of Mg.

To obtain information on the compensation level of Mg by the vacancy cluster, we assume that the vacancy cluster is decorated by Mg impurities as demonstrated by the TEM results of the pyramidal defects. The cluster concentration is obtained from the positron experiments (Table II), and we approximate the maximum passivation effect by assuming that the internal surface of the vacancy cluster is totally covered by Mg atoms. As a result one can deduce that one cluster with a radius of  $r = 5 \text{ \AA}$  can bind a maximum of 100 Mg atoms, which leads to the compensation level of  $4.5 \times 10^{17} \text{ cm}^{-3}$ . Hence, the total compensation effect by vacancy defects is less than  $10^{18} \text{ cm}^{-3}$ , which is up to 30 % of the total amount of electrically deactivated Mg. The hydrogen passivation thus seems to be dominant mechanism, but the vacancy defect may explain the additional electrical deactivation of Mg acceptors.

## B. Annealing effects

### 1. Annealing of the vacancy clusters

The results presented here show that the vacancy cluster of about 60 atoms is replaced by smaller clusters during the thermal annealing process. The vacancy cluster consists of vacancies in both sublattices, and the dissociation is a matter of binding energy and the diffusion barrier of the individual monovacancy. According to theory and experimental results<sup>5,6</sup>, the migration barriers of vacancy defects are 3.96 eV, 2.65 and 1.9 for  $V_N^{+1}$ ,  $V_N^{+3}$  and  $V_{Ga}^{-3}$ , respectively. The vacancy cluster may thus recover in the following way: At high temperature the cluster dissociates into monovacancies, which diffuse rapidly in the material. The diffusion of monovacancies is slowed down by encountering a vacancy in the opposite sublattice, leading to the formation of smaller vacancy clusters either at the annealing temperature or during cooling down process.

The activation energy of cluster dissociation can be roughly estimated. We use the expression of  $N = \omega t e^{-E_A/k_b T}$ , where N is the number of jumps of individual defect in a given lattice, t is the annealing time and T temperature. A prefactor value of  $\omega = 1 \times 10^{13} \text{ s}^{-1}$  yields typical value for a jump frequency. In order to dissociate a cluster the required number of jumps could be between 1 and 100. In the case of RTA ( $t \approx 100\text{s}$ ) at 1000 °C we have  $E_A = 3.3\text{-}3.8 \text{ eV}$ . This value is larger than the theoretical and experimental values for the migration of  $V_N^{+3}$  (2.6 eV) and  $V_{Ga}$  (1.8 eV). Assuming these migrating species, we estimate the binding energy of the vacancy cluster in the order of 1 - 2 eV.

The PL spectra of samples with high concentration of Mg acceptors show typically, after thermal annealing, emission bands with peaks in the spectral region between 2.7 and 2.9 eV.<sup>12</sup> This coincides with the appearance of the Ga vacancy related small-clusters formed after the thermal annealing induced dissociation of the larger clusters. The observed vacancy clusters are positron traps in both the neutral and the negative charge states. Associating these defects with the 2.7 - 2.9 eV emission bands is attractive, but a detailed PL study is necessary to establish this identification.

### 2. Annealing of the $V_N\text{-Mg}_{Ga}$ pair

The pairs of N vacancy and Mg dopants are observed here as well as in our previous work.<sup>10</sup> In the present experiments no evidence of  $V_N\text{-Mg}_{Ga}$  defects are observed after annealing, and our previous results indicate that the concentration of these pairs decreases with annealing between 500 and 800 C. Since these defects are not observed in MBE samples, which does not require post-growth thermal annealing to activate the Mg acceptors, we infer that the  $V_N\text{-Mg}_{Ga}$  complexes are stable in semi-insulating GaN but unstable in p-type materials. During

annealing GaN is converted to p-type, mainly by the removal of the passivating hydrogen and by the dissociation of the  $V_N$ -Mg<sub>Ga</sub> pairs and migration of  $V_N$ . We estimate the migration barrier of  $V_N$  as 2.5(3) eV,<sup>10</sup> which is close to the calculated value of  $V_N^{+3}$ .<sup>5,6</sup> In fact, the calculations explain the different stabilities of  $V_N$ -Mg<sub>Ga</sub> complexes in p-type and semi-insulating GaN, since the large migration barrier of  $V_N^{+1}$  of 3.96 eV makes the  $V_N$ -Mg<sub>Ga</sub> complex very stable when the Fermi level is at midgap.

Recently Wright and Mattsson<sup>6</sup> have calculated the migration barriers of  $V_N$  related defects, with similar results as found by Limpijumng and Van de Walle.<sup>5</sup> Wright and Mattsson further analyzed our positron annihilation experiments<sup>10</sup>. According to their theory, the  $V_N$  left from the dissociating  $V_N$ -Mg<sub>Ga</sub> complex is able to migrate to the surface during 800 °C annealing. Diffusion length of about 6 Å was estimated for  $V_N$  during 500 °C annealing. This is in good agreement with our results at this annealing temperature, where a clear decrease of  $V_N$ -Mg<sub>Ga</sub> concentration was observed.<sup>10</sup> Notice that a small diffusion length of 6 Å is enough to remove the positron trapping at the  $V_N$ -Mg<sub>Ga</sub> complex, since the isolated  $V_N^{+3}$  or  $V_N^{+1}$  can not be observed by positron annihilation spectroscopy due to Coulomb repulsion. Furthermore, reduced positron trapping at  $V_N$ -Mg<sub>Ga</sub> pairs is still observed in annealed (500 - 800 °C) samples,<sup>10</sup> which already show p-type conductivity ( $p = 3 \cdot 10 \times 10^{16} \text{ cm}^{-3}$ ). This implies that (i) some of the  $V_N$ -Mg<sub>Ga</sub> complexes survive the annealing, and (ii) at least a fraction of the  $V_N$ -Mg<sub>Ga</sub> complexes remain in neutral charge state even in p-type GaN, since they are observed as positron traps.

The works of Lee *et al.* and Wright and Mattsson point out the hydrogen decoration of  $V_N$  related complexes such as  $V_N$ -Mg<sub>Ga</sub><sup>6</sup> or  $V_N$ -Mg<sub>i</sub>.<sup>40</sup> While we agree that such complexing may be possible, we do not think that  $V_N$ -Mg<sub>Ga</sub>-H complexes would trap positrons, since the presence of H decreases the open volume and increases the positive charge of the complex. The removal of H from  $V_N$ -Mg<sub>Ga</sub>-H complexes during annealing would in-

crease the positron trapping at  $V_N$  defects, which contradicts our experimental observation. Therefore, we believe that the  $V_N$ -Mg<sub>Ga</sub> defects observed in the present or in the previous work<sup>10</sup> are unlikely to be decorated with hydrogen.

## V. CONCLUSION

We have studied Mg doped GaN films with positron annihilation spectroscopy to find out the effect of Mg doping, Si codoping and thermal annealing on open volume defects. Vacancy related defects are observed only for Mg doping levels of about  $10^{19} \text{ cm}^{-3}$ . Studies of unannealed GaN:Mg sample resulted on the detection of two vacancy defects; one with a positron lifetime of 180 ps and another with a lifetime of 435 ps. They are identified as  $V_N$ -Mg<sub>Ga</sub> and vacancy clusters, respectively.

The vacancy clusters have an inhomogeneous depth profile in the unannealed GaN:Mg, typically a lower concentration down to 300-500 nm from the surface. The concentration of  $V_N$ -Mg<sub>Ga</sub> changes less throughout the layer. Annealing dissociates  $V_N$ -Mg<sub>Ga</sub>-pairs as well as the vacancy clusters, which leads to an uniform vacancy distribution through the film. The vacancy defect formed by the dissociated vacancy clusters is identified as a Ga vacancy related smaller cluster. The samples co-doped with Si donors show similar behavior as that observed in the samples doped only with Mg.

Before annealing the concentration of  $V_N$ -Mg<sub>Ga</sub> is estimated of  $2 \cdot 3 \times 10^{17} \text{ cm}^{-3}$  while the vacancy cluster concentration varies between  $0.5 \cdot 5 \times 10^{15} \text{ cm}^{-3}$ , with a region of lower concentration just below surface. These defects are important for the compensation of Mg acceptors in GaN. The quantitative estimates presented here, however, suggest that the hydrogen passivation of Mg is the dominant deactivation mechanism.

We thank Prof. M. J. Puska for his help in the theoretical calculations of positron lifetimes at vacancy clusters.

---

\* On leave from KFKI Central Research Institute for Nuclear and Particle Physics, H-1525 Budapest P.O.B. 49, Hungary  
<sup>1</sup> S. Nakamura, T. Mukai, M. Senoh, and N. Iwasa, Jpn. J. Appl. Phys. **31**, L139 (1992).  
<sup>2</sup> H. Amano, M. Kito, K. Hiramatsu, and I. Akasaki, Jpn. J. Appl. Phys. **28**, L2112 (1989).  
<sup>3</sup> U. Kaufmann, M. Kunzer, M. Maier, H. Obloh, A. Ramakrishnan, B. Santic, and P. Schlotter, Appl. Phys. Lett. **72**, 1326 (1998).  
<sup>4</sup> I. Gorczyca, A. Svane, and N. E. Christensen, Phys. Rev. B **61**, 7494 (2000).  
<sup>5</sup> S. Limpijumng and C. G. Van de Walle, Phys Rev. B **69**, 035207 (2004).  
<sup>6</sup> A. F. Wright and T. R. Mattsson, J. Appl. Phys. **96**, 2015 (2004).

<sup>7</sup> Z. Liliental-Weber, M. Benamara, W. Swider, J. Washburn, I. Grzegory, and S. Porowski, Phys. Rev. Lett. **83**, 2370 (1999).

<sup>8</sup> Z. Liliental-Weber, M. Benamara, W. Swider, J. Washburn, I. Grzegory, S. Porowski, D. J. H. Lambert, C. J. Eiting, and R. D. Dupuis, Appl. Phys. Lett. **75**, 4159 (1999).

<sup>9</sup> R. Krause-Rehberg and H. S. Leipner, *Positron annihilation in semiconductors* (Springer-Verlag, Berlin, 1999).

<sup>10</sup> S. Hautakangas, J. Oila, M. Alatalo, K. Saarinen, L. Liskay, D. Seghier, and H. P. Gislason, Phys. Rev. Lett. **90**, 137402 (2003).

<sup>11</sup> Jeremy Moxom, Jun Xu, R. Suzuki, T. Ohdaira, George Brandes and Jeffrey S. Flynn, J. appl. Phys. **92**, 1898 (2002).

- <sup>12</sup> E. R. Glaser, W. E. Carlos, G. C. B. Braga, J. A. Freitas, Jr., W. J. Moore, B. V. Shanabrook, R. L. Henry, A. E. Wickenden, D. D. Koleske, H. Obloh, P. Kozodoy, S. P. DenBaars, and U. K. Mishra, *Phys. Rev. B* **65**, 085312 (2002).
- <sup>13</sup> P. Laukkanen, S. Lehtonen, P. Uusimaa, M. Pessa, J. Oila, S. Hautakangas, K. Saarinen, J. Likonen, and J. Keränen, *J. Appl. Phys.* **92**, 786 (2002).
- <sup>14</sup> M. A. Reshchikov, G.-C. Yi, and B. W. Wessels, *Phys. Rev. B* **59**, 13176 (1999).
- <sup>15</sup> H. Teisseyre, T. Suski, P. Perlin, I. Grzegory, M. Leszczynski, M. Bockowski, S. Porowski, J. A. Freitas, Jr., R. L. Henry, A. E. Wickenden, and D. D. Koleske, *Phys. Rev. B* **62**, 10151 (2000).
- <sup>16</sup> K. Saarinen, P. Seppälä, J. Oila, P. Hautojärvi, C. Corbel, O. Briot and R. L. Aulombard, *Appl. Phys. Lett.* **73**, 3253 (1998).
- <sup>17</sup> K. Saarinen, P. Hautojärvi and C. Corbel, *Identification of Defects in Semiconductors* (Academic, New York, 1998).
- <sup>18</sup> J. Oila, V. Ranki, J. Kivioja, K. Saarinen, P. Hautojärvi, J. Likonen, J. M. Baranowski, K. Pakula, T. Suski, M. Leszczynski, and I. Grzegory, *Phys. Rev. B* **63**, 045205 (2001).
- <sup>19</sup> J. Oila, K. Saarinen, A. E. Wickenden, D. D. Koleske, R. L. Henry and M. E. Twigg, *Appl. Phys. Lett.* **82**, 1021 (2003).
- <sup>20</sup> K. Saarinen, T. Laine, S. Kuisma, J. Nissilä, P. Hautojärvi, L. Dobrzynski, J. M. Baranowski, K. Pakula, R. Stepniewski, M. Wojdak, A. Wyszomolek, T. Suski, M. Leszczynski, I. Grzegory, and S. Porowski, *Phys. Rev. Lett.* **79**, 3030 (1997).
- <sup>21</sup> E. Calleja et al., *Phys. Rev. B* **58**, 1550 (1998).
- <sup>22</sup> These calculations are based on generalized gradient approximation (GGA) for positron-electron correlation.
- <sup>23</sup> R. M. Nieminen, J. Laakkonen, P. Hautojärvi, and A. Vehanen, *Phys. Rev. B* **19**, 1397 (1979).
- <sup>24</sup> T. E. M. Staab, M. Haugk, T. Frauenheim, H. S. Leipner, *Phys. Rev. Lett.* **83**, 5519 (1999).
- <sup>25</sup> M. J. Puska and R. M. Nieminen, *J. Phys. F* **13**, 333 (1983).
- <sup>26</sup> M. J. Puska and R. M. Nieminen, *Rev. Mod. Phys.* **66**, No. 3, (1994).
- <sup>27</sup> E. Boronski and R. M. Nieminen, *Phys. Rev. B* **34**, 3820 (1986).
- <sup>28</sup> W. Brandt and J. Reinheimer, *Phys. Lett. A* **35**, 109 (1971).
- <sup>29</sup> R. Krause-Rehberg, H. S. Leipner, A. Kupsch, A. Polity, and Th. Drost, *Phys. Rev. B* **49**, 2385 (1994).
- <sup>30</sup> R. Krause-Rehberg, M. Brohl, H. S. Leipner, Th. Drost, A. Polity, U. Beyer, and H. Alexander, *Phys. Rev. B* **47**, 13266 (1993).
- <sup>31</sup> M. J. Puska, C. Corbel, and R. M. Nieminen, *Phys. Rev. B* **41**, 9980 (1990).
- <sup>32</sup> W. Götz, N. M. Johnson, D. P. Bour, M. D. McCluskey and E. E. Haller, *Appl. Phys. Lett.* **69**, 3725 (1996).
- <sup>33</sup> B. Clerjaud, D. Côte, A. Lebkiri, C. Naud, J. M. Baranowski, K. Pakula, D. Wasik, and T. Suski, *Phys. Rev. B* **61**, 8238 (2000).
- <sup>34</sup> S. Limpijumng, J. E. Northrup, and C. G. Van de Walle, *Phys. Rev. B* **68**, 075206 (2003).
- <sup>35</sup> Z. Liliental-Weber, Y. Chen, S. Ruvimov, and J. Washburn, *Phys. Rev. Lett.* **79**, 2835 (1997).
- <sup>36</sup> Z. Liliental-Weber, T. Tomaszewicz, D. Zakharov, J. Jasinski, and M. A. O'Keefe, *Phys. Rev. Lett.* **93**, 206102 (2004).
- <sup>37</sup> Z. Liliental-Weber, T. Tomaszewicz, D. Zakharov, J. Jasinski, M.A. O'Keefe, S. Hautakangas, A. Laakso, and K. Saarinen, *Mat. Res. Soc. Symp. Proc.* **798**, Y9.7.1 (2004).
- <sup>38</sup> B Santic, *Semicond. Sci. Technol.* **18**, 219 (2003).
- <sup>39</sup> We use the basic approach for the approximation of the Fermi level in a non-degenerate semiconductor material
- $$[N_a - N_d] = N_v e^{-(E_F - E_V)/k_b T}, \quad (7)$$
- where  $N_v = 2(2\pi m_h k_b T / \hbar^2)$ . The concentration of activated acceptors is  $[N_a^-] = [Mg] f(E_a)$ , where  $f(E_a)$  is the Fermi function.
- <sup>40</sup> S.-G. Lee and K. J. Chang, *Semicond. Sci. Technol.* **14**, 138 (1999).